ACS APPLIED MATERIALS & INTERFACES

www.acsami.org

Research Article

Highly Stretchable Printed Poly(vinylidene fluoride) Sensors through the Formation of a Continuous Elastomer Phase

Ruowen Tu and Henry A. Sodano*

Cite This: *ACS Appl. Mater. Interfaces* 2023, 15, 22320−22331

Read Online

ACCESS | Metrics & More | Article Recommendations | Supporting Information

ABSTRACT: Stretchable piezoelectric stress/strain sensing materials have attracted substantial research interest in the fields of wearable health monitoring, motion capturing, and soft robotics. These sensors require operation under dynamic loading conditions with high strain range, changing strain/loading rates, and varying pre-stretch states, which are challenging conditions for existing sensors to produce reliable measurements. To overcome these challenges, an intrinsically stretchable poly(vinylidene fluoride) (PVDF) sensor is developed through the polymer blending of PVDF and acrylonitrile butadiene rubber (NBR). Through precipitation printing and vulcanization, the resulting PVDF/NBR blends exhibit strong β phase PVDF and a blend morphology with submicron-level phase separation, but also strains up to 544%. Both the blend morphology and the mechanical properties indicate that this PVDF/NBR blend can be considered as a continuous elastomer phase above micron scale. After electric poling and adding electrodes, the PVDF/NBR blends have excellent piezoelectric properties to be used as both stretching mode strain sensors and compression mode stress/force sensors. The stretching mode sensors can measure strain up to 70% without strain rate and pre-stretch dependence, while the compression mode sensors have a loading-rate-independent linear voltage−stress relationship up to 4.8 MPa stress and a negligible pre-stretch dependence. Therefore, the PVDF/NBR sensors can provide accurate and reliable stress/strain measurements when attached to soft structures, which paves the way for sensing and calibration of soft robots under dynamic loading conditions.

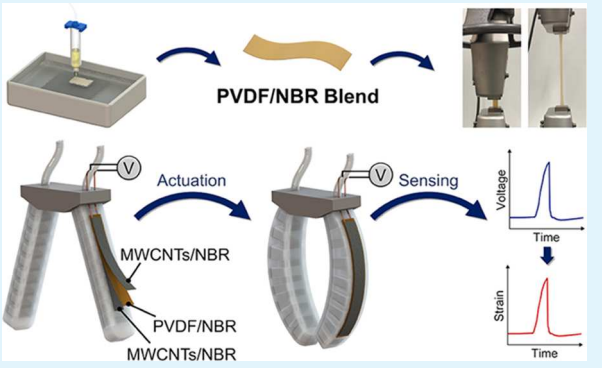

KEYWORDS: *stretchable, piezoelectric, polymer blends, sensing, dynamic loading*

1. INTRODUCTION

Stress and strain sensing using multifunctional materials is one of the key functions of smart structures to achieve structural health monitoring, deformation measurement, and actuator calibration and control. Flexible and stretchable stress/strain sensing materials have gained substantial research interest over the past decade due to the development of wearable electronics for biomedical applications,[1,2] biomechanical study,[3] motion capture technology,[4] and soft robotics.[5] Based on the sensing mechanism, stress/strain sensing materials have three main categories: capacitive, piezoresistive, and piezoelectric.[6] Among the three, piezoelectric materials have excellent sensing linearity, ultralow response time, and no intrinsic power consumption, which are suitable for dynamic sensing applications. However, since most piezoelectric materials are nearly inextensible, many research studies on stretchable piezoelectric devices focus on pattern design that can improve the device stretchability by using meshes,[7] wavy shapes,[8,9] serpentine interconnects,[10,11] and kirigami designs.[12,13] For example, Duan et al. used direct ink writing of poly(vinylidene fluoride) (PVDF) fiber on pre-stretched poly(dimethylsiloxane) (PDMS) to produce in-plane wavy piezoelectric structures that were able to measure in-plane deformation up to 110% strain.[9] Ji and Zhang showed a serpentine patterned PVDF sensor with stretchability up to 35% and a voltage sensitivity of 0.97 mV $\mu\varepsilon^{-1}$ that could monitor respiratory and heartbeat signals in real time.[11] Kim et al. developed piezoelectric strain sensors with stretchability up to 320% based on kirigami designs, which were demonstrated on virtual reality haptic gloves for finger motion sensing.[12] Although creative pattern design allows for high device stretchability using inextensible piezoelectric materials, complex geometries also cause limitations such as calibration difficulty, high strain rate dependence, and short fatigue life at the joints.

Developing new piezoelectric materials with intrinsic stretchability is the other approach for stretchable piezoelectric sensors, which can be combined with smart pattern designs to further boost the device stretchability. The main type of

Received: January 25, 2023
Accepted: April 11, 2023
Published: April 29, 2023

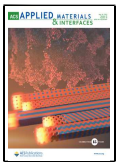

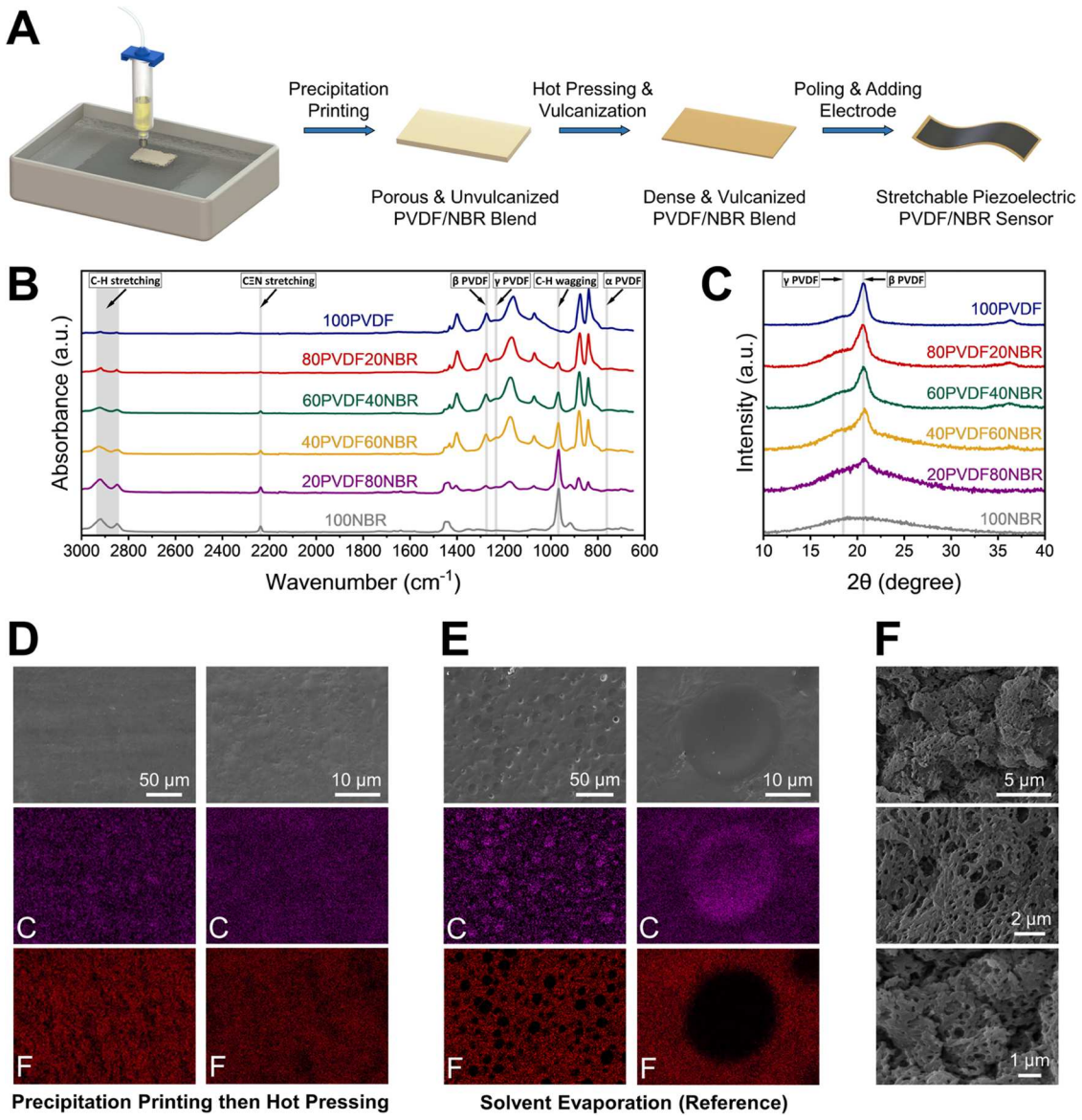

Figure 1. Fabrication process and characterization of PVDF/NBR blends. (A) Fabrication process of PVDF/NBR sensors. (B) FTIR spectra of PVDF/NBR blends. (C) XRD patterns of PVDF/NBR blends. (D) SEM images and EDS mappings of PVDF/NBR blend formed by precipitation printing and hot pressing (60PVDF40NBR as an example). (E) SEM images and EDS mappings of reference 60PVDF40NBR blend formed by solvent evaporation. (F) SEM images of hot DMF-etched precipitation-printed then hot-pressed 60PVDF40NBR, where the remaining continuous phase is NBR.

stretchable piezoelectric materials are nanocomposites that consist of piezoelectric nanofillers and an elastomer matrix.[14−17] Chou et al. mixed 65 vol % lead zirconate titanate (PZT) particles into silicone rubber and showed that the nanocomposite had a high open-circuit voltage output of 20 V and up to 200% stretchability, allowing it to be used for energy harvesters or stretchable load sensors.[18] Similarly, Quinsaat et al. developed elastic piezoelectric nanocomposites of 38 vol % PZT in a PDMS matrix with d_{33} = 3.6 pC N^{-1}, d_{31} = −30 pC N^{-1}, and a strain at break of 254%, which was used as a compression detection sensor.[19] Although nanocomposites with piezoelectric ceramic fillers generally have high voltage outputs, poor sensing performance under high strain (>50%) can be expected due to the significant difference in modulus between the matrix and filler, which results in low stress transfer efficiency, slip, and interfacial failure. Another type of stretchable piezoelectric materials are sandwich composites, which contain a piezoelectric center layer sandwiched by two elastomer shell layers. Electrospun PVDF and its copolymer poly(vinylidene fluoride)-co-trifluoroethylene (PVDF-TrFE) are popular piezoelectric layer materials for the sandwich composite due to their convenient self-polarized electrospinning process.[20] Thus, researchers have developed flexible sandwich composites consisting of electrospun PVDF-TrFE embedded in PDMS for high-resolution pressure sensing applications.[21,22] However, most PVDF-based sandwich composites have limited stretchability (∼30%) and cannot be used in applications that require large extension.

With the recent development of soft robotics, strain/stress sensors used on soft actuators and passive structures that require a large strain sensing range (>50%) under dynamic loading conditions are in great demand. When under dynamic loading conditions, the strain/loading rates of the soft structures can change and the pre-stretch strain of the quasi-static states may

https://doi.org/10.1021/acsami.3c01168
ACS Appl. Mater. Interfaces 2023, 15, 22320−22331

vary, which are challenging for existing stretchable piezoelectric sensors to produce reliable strain/stress measurements. To overcome these limitations of sensors based on either smart pattern design or piezoelectric composites, intrinsically stretchable piezoelectric materials in the form of polymer blends with tailored macroscopically uniform properties can be developed. Polymer blends containing the polar β phase PVDF have been widely studied as piezoelectric films and nanofibers, such as PVDF/poly(methyl-methacrylate) (PMMA),[23−25] PVDF/poly(vinyl alcohol) (PVA),[26] PVDF/thermoplastic polyurethane (TPU),[27] and PVDF/photopolymers,[28] and their piezoelectric properties and stretchability are compared in Table S1. In particular, for stretchable sensor materials, PVDF/acrylonitrile butadiene rubber (NBR) blend can be a potential candidate that possesses both stretchability and piezoelectricity. Researchers have shown that the PVDF/NBR blend formed by melt mixing is a compatible polymer blend that has excellent toughness and stretchability, while vulcanization of the NBR phase can further stabilize the blend morphology and improve the interfacial bonding between phases.[29,30] However, the potential of using PVDF/NBR blend as a stretchable piezoelectric material has not been explored. In this research, PVDF/NBR blends were formed using a precipitation printing method, where a solution of both PVDF and unvulcanized NBR dissolved in *N*,*N*-dimethylformamide (DMF) are precipitated inside a water bath and solidified as polymer blends that can be vulcanized by subsequent hot pressing.[31] This polymer blending method was inspired by previous studies that have shown the promotion of β phase PVDF for piezoelectricity through solvent exchange and phase inversion of the PVDF/DMF/water system.[32−35] Therefore, phase composition, blend morphology, piezoelectric properties, and stretchability of the precipitation-printed then hot-pressed PVDF/NBR blends were characterized in this paper as the fundamentals for stretchable sensor applications. In addition, the developed piezoelectric PVDF/NBR sensors have been verified to have reliable and accurate strain/stress sensing performance in a large strain range with negligible strain/loading rate and pre-stretch dependence, which can overcome some limitations of existing stretchable strain/stress sensors under dynamic loading conditions.[13,19,36−42]

2. RESULTS AND DISCUSSION

2.1. Fabrication of PVDF/NBR Blends. Four different weight ratios of the PVDF/NBR printing inks (20PVDF80NBR, 40PVDF60NBR, 60PVDF40NBR, 80PVDF20NBR, where the number in front of each polymer component is its weight percent out of total solid) along with neat PVDF (100PVDF) and neat NBR (100NBR) inks were obtained by dissolving the corresponding polymers and vulcanization agents in DMF to form 15 wt % solutions. The polymer inks were then precipitation-printed in a water bath to produce thick films (ca. 0.2−1.5 mm thickness) of unvulcanized PVDF/NBR blends using a solution dispensing three dimensional (3D) printer (Figures 1A and S1). Based on literature studies and our own experiments, lower water bath temperature promotes polar β phase formation during the precipitation process (Figure S2 and Section 2.2 in the Supporting Information).[33,34,43,44] By considering both β phase formation and printability, 0 °C ice/water mixture was selected as the printing bath. After precipitation printing, unvulcanized PVDF/NBR blends were hot-pressed at 150 °C, which was also optimized for β phase preservation (Figure S3 and Section 2.3 in the Supporting Information) to induce vulcanization and reduce porosity.

2.2. Characterization of PVDF/NBR Blends. The chemical structure of the precipitation-printed and hot-pressed PVDF/NBR blends was investigated through Fourier transform infrared (FTIR) spectroscopy, and the resulting spectra of six different mixing ratio samples are shown in Figure 1B. The intensity of C−H stretching absorption band increases as the NBR amount increases, which is attributed to the methylene group of the butadiene part (symmetrical stretching at 2850 cm^{-1} and asymmetrical stretching at 2920 cm^{-1}). Similar increasing trends can also be seen at 2237 and 968 cm^{-1}, which are C≡N stretching of the acrylonitrile part and C−H wagging of the trans-1,4-structure of the butadiene part. The crystalline phases of PVDF can be determined by the characteristic peaks of α, β, and γ phases. For all samples that contain PVDF, no clear α phase peak at 762 cm^{-1} can be seen, yet an intense β phase peak at 1275 cm^{-1} and a γ phase shoulder at 1234 cm^{-1} can be clearly observed. The quantitative phase fraction calculation based on the FTIR absorption peaks in Table S2 also shows that up to 88.2% β phase fraction can be achieved in PVDF/NBR. This means the prepared PVDF/NBR blends have dominant polar β phase and some extent of less polar γ phase in the crystalline region of PVDF, which provides the chemical structure basis of piezoelectricity. The crystalline phases of the PVDF/NBR blend can be further verified through X-ray diffraction (XRD), which is presented in Figure 1C. All samples with PVDF content exhibit a main β phase peak around 2θ = 20.7° (200/110) and a γ phase shoulder at 2θ = 18.5° (020), while no clear α phase peak at 2θ = 17.6° (100) and 19.9° (021) can be seen.[45−47] As an amorphous polymer, 100NBR only shows an amorphous dome without any diffraction peak. Moreover, by using differential scanning calorimetry (DSC) to study the melting and glass transition behaviors (Figures S4 and S5, Table S3), the PVDF/NBR blend is found to be an immiscible (heterogeneous) polymer blend with three phases: crystalline PVDF, amorphous PVDF, and amorphous NBR.

To further study the morphology of the PVDF/NBR blends, scanning electron microscopy (SEM) and energy-dispersive X-ray spectroscopy (EDS) were performed on the surfaces of PVDF/NBR films. Figures S6−S11 show the large-area SEM images and EDS mappings of the chemical elements C, F, N, and S, where uniformly distributed PVDF (F mapping), NBR (N mapping), and sulfur (S mapping) are observed for all PVDF/NBR blends. Higher-magnification SEM images and EDS mappings in Figure 1D show a unique blend morphology of the surface of the PVDF/NBR formed by precipitation printing then hot pressing (60PVDF40NBR as an example). Unlike the surface of the reference 60PVDF40NBR blend formed by casting then solvent evaporation that has large NBR craters (diameters of 10−20 μm) in Figure 1E, the 60PVDF40NBR produced by precipitation printing then hot pressing in this work has a submicron-level phase separation which remains stable after vulcanization. The mechanism of this polymer blend morphology formation is similar to the widely studied immersion precipitation method to produce porous membranes, where the DMF has nearly instantaneous diffusion into water to facilitate solvent exchange while NBR and PVDF nucleate simultaneously without enough time and mobility for polymer−polymer diffusion.[48] The lack of polymer−polymer diffusion allows the precipitation-printed PVDF/NBR blend to keep a submicron-level demixing of PVDF and NBR without NBR phase coarsening like cast PVDF/NBR films. To have a better

https://doi.org/10.1021/acsami.3c01168
ACS Appl. Mater. Interfaces 2023, 15, 22320−22331

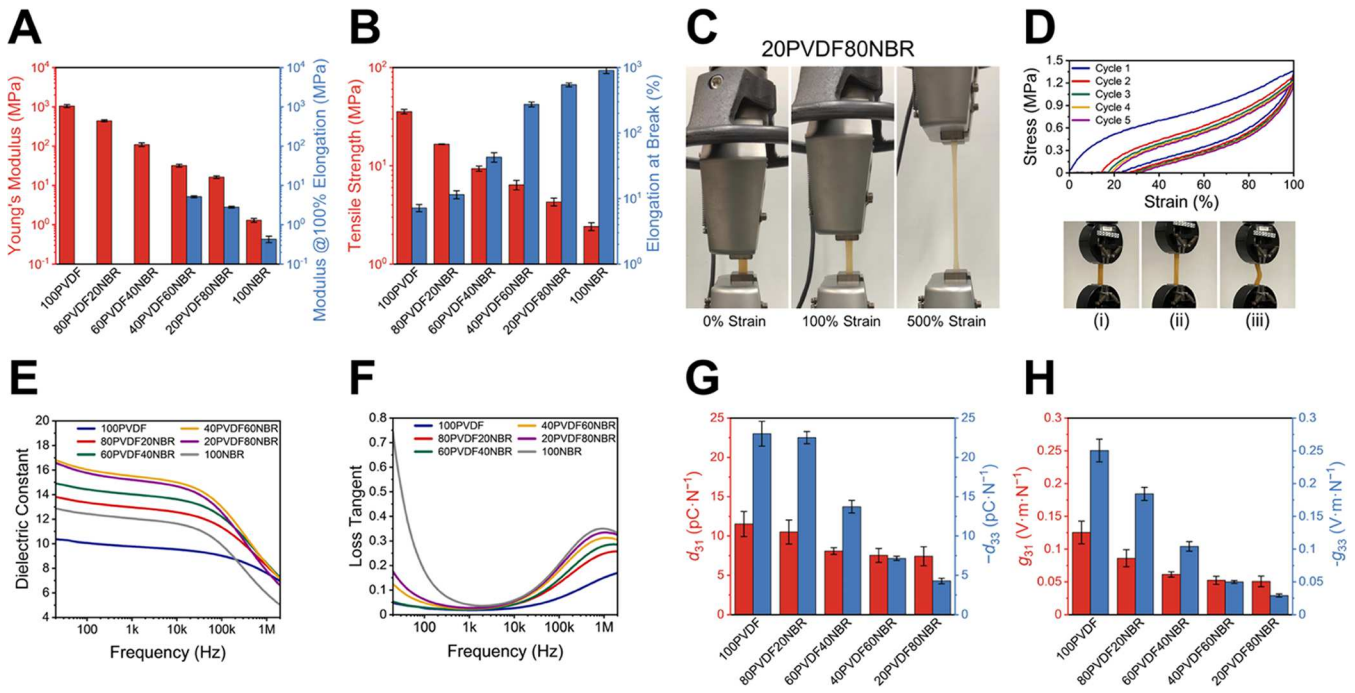

Figure 2. Mechanical, dielectric, and piezoelectric properties of PVDF/NBR blends. (A) Young's modulus and modulus at 100% elongation of the different blends. (B) Tensile strength and elongation at break of the different blends. (C) Stretchability of a 20PVDF80NBR sample. (D) Five consecutive loading−unloading cycles of a 20PVDF80NBR sample and the three stages of the first loading−unloading cycle: (i) initial state, (ii) peak strain state, (iii) unloaded state. (E) Dielectric constant of different blends with respect to frequency. (F) Loss tangent of different blends with respect to frequency. (G) Piezoelectric charge coefficients of the different blends. (H) Piezoelectric voltage coefficients of the different blends.

understanding of the blend morphology, the precipitation-printed then hot-pressed 60PVDF40NBR is also etched by hot DMF to remove the PVDF phases. The resulting surfaces in Figure 1F show that the remaining crosslinked NBR phase has a continuous and highly interlocked morphology with removed PVDF pores, but the average size of the PVDF phase cannot be determined due to the swelling of NBR after DMF etching. In addition, more SEM images and EDS mappings of the surfaces and tensile fracture cross sections of different blend ratios in Figures S12−S14 further support the submicron-level phase separation. Therefore, the precipitation-printed then hot-pressed PVDF/NBR can be considered as a continuous elastomer phase above the micron level, which is different from typical two-phase piezoelectric nanocomposites with phase sizes from several to tens of microns.[16,18,49]

2.3. Mechanical, Dielectric, and Piezoelectric Properties. The mechanical properties of the PVDF/NBR blends were tested through tensile testing and are shown in Figure 2A,B. In Figure 2A, the Young's modulus drops significantly from 1045 MPa (100PVDF) to 16.2 MPa (20PVDF80NBR) as the NBR weight fraction increases, and the modulus at 100% elongation of 20PVDF80NBR is only 2.8 MPa. Similarly, the tensile strength of the blends decreases as the NBR weight fraction increases (Figure 2B). However, the addition of NBR provides exceptional stretchability to the blend. The average elongation at break increases from 7% (100PVDF) to 544% (20PVDF80NBR), which is attributed to the high elongation (902%) of neat NBR. The stretchability of PVDF/NBR blend using 20PVDF80NBR as the example is demonstrated in Figure 2C and a tensile test video (Movie S1). Figure 2D shows the stress−strain curves of a 20PVDF80NBR sample under 100% strain cyclic loading with a 0.1 s^{-1} strain rate. After the first loading−unloading cycle, the 20PVDF80NBR sample had about 25% remaining strain, which mainly came from its viscoelasticity and plastic deformation from the PVDF phase due to its low yield strain.[31,50] However, after the PVDF phase was plastically deformed, the following four consecutive cycles had almost identical stress−strain curves, lower hysteresis, and lower peak stress compared to the first cycle. The remaining strain in these four cycles was only caused by the time-dependent viscoelasticity, which could be recovered if given enough settling time. Thus, preconditioning of the PVDF/NBR sensor before application by stretching through the operating strain range and then releasing is a simple and effective approach to improve repeatability and reduce the hysteresis of this material (Figure S15). It has also been shown that the viscoelastic hysteresis is strain-rate-dependent, which reduces as the strain rate increases (Supporting Information Section 7.3). Therefore, to be used as a stretchable sensing material, high-NBR-content PVDF/NBR exhibits high elongation, consistent stress−strain curves under cyclic loading, and low hysteresis under high strain rates, which is highly desirable for dynamic sensing conditions.

The dielectric properties of the PVDF/NBR blends are measured in the frequency range from 20 Hz to 2 MHz. In Figure 2E, the dielectric constant of all blends drops as the frequency increases, while the drop above 100 kHz is more significant with higher NBR content. In addition, we noticed an abnormal phenomenon that the dielectric constant of the PVDF/NBR blend is higher than both neat PVDF and NBR (Figure S16a). This phenomenon has been previously discovered for other polymer blends, where the nanoscale mixing of two dipolar polymers can slightly increase the chain spacing and thus reduce the dipole reorientation barriers.[51] In Figure 2F, the loss tangent curves of the blends show an α relaxation that moves toward the lower frequency and has a

https://doi.org/10.1021/acsami.3c01168
ACS Appl. Mater. Interfaces 2023, 15, 22320−22331

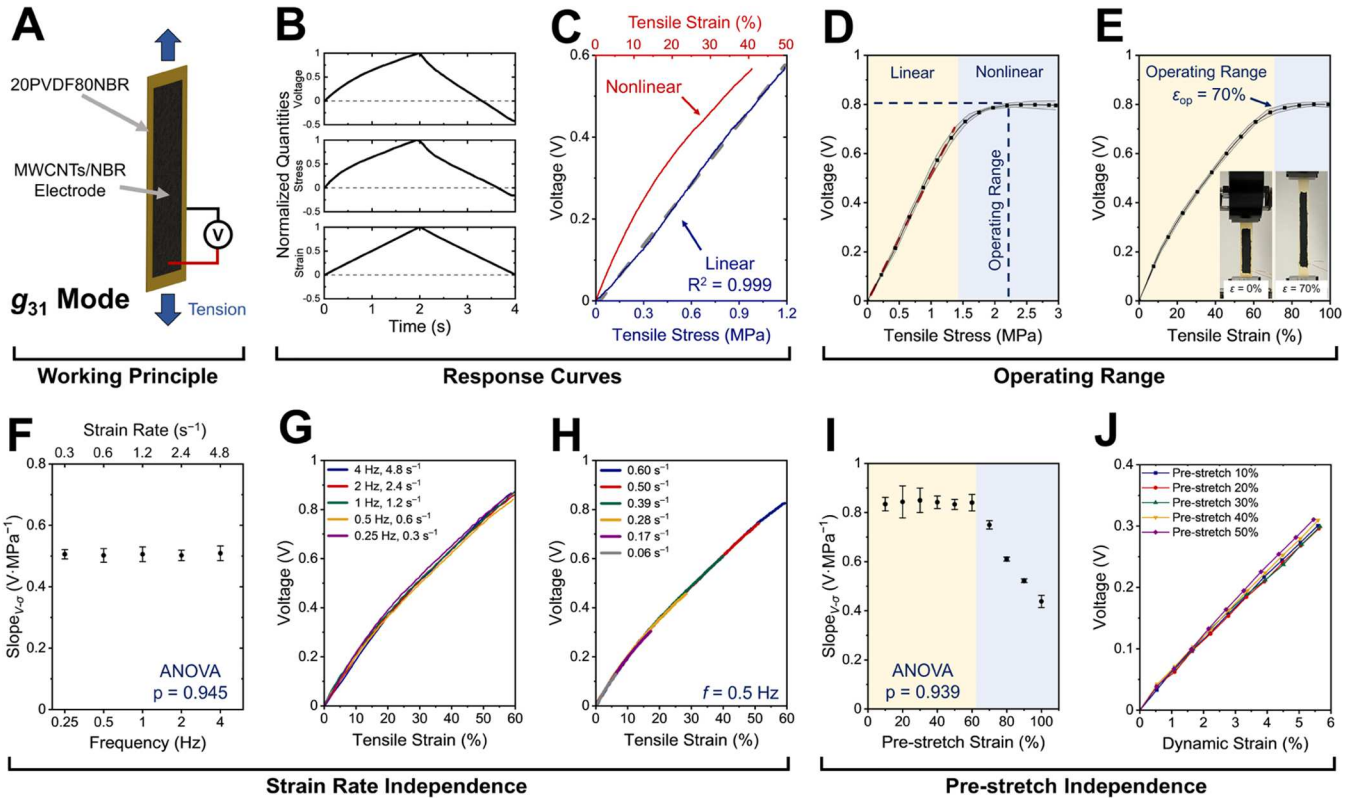

Figure 3. Characterization of the stretching mode 20PVDF80NBR sensors. (A) Schematic of its working principle. (B) Normalized voltage and stress response to a triangle strain excitation. (C) Voltage−stress response with a linear fit and nonlinear voltage−strain response. (D) Linear range and operating range of the voltage−stress curve with error bands. (E) Operating range of the voltage−strain curve with error bands. (F) Frequency-independent and strain-rate-independent voltage−stress slopes. (G) Frequency-independent and strain-rate-independent voltage−strain curves up to 60% strain. (H) Strain-rate-independent voltage−strain curves with various strain amplitude excitations at 0.5 Hz. (I) Effect of pre-stretch strain on dynamic stress sensing. (J) Effect of pre-stretch strain (10−50%) on dynamic strain sensing.

higher peak value with an increasing amount of NBR.[52] The loss tangent on the low-frequency end (Figure S16b) has a dramatic increase as the NBR content increases, which can be explained by the Maxwell-Wagner polarization of heterogeneous materials. The high loss tangent of NBR attributes to the dielectric constant difference between the NBR and remaining sulfur or accelerator that induces interfacial charges.[53]

The longitudinal and transverse piezoelectric properties of the blends after electric poling are shown in Figure 2G,H. By using a 0/90° alternating infill pattern for precipitation printing, PVDF/NBR blends are expected to have transversely isotropic piezoelectric properties, which has been verified for 100PVDF (Figure S17). Thus, d_{31} and g_{31} are measured to represent the transverse piezoelectric properties, and the piezoelectric properties of 100PVDF and commercial stretched PVDF films are compared in Table S4. In Figure 2G, both piezoelectric charge coefficients d_{31} and d_{33} decrease as the PVDF content reduces, yet the decrease in d_{33} is more significant than d_{31}. Similarly, after considering the dielectric constant of the blends, the piezoelectric voltage coefficient g_{33} in Figure 2H has a steeper drop than g_{31} as the PVDF weight fraction decreases, due to the anisotropy between the longitudinal and transverse modulus of the hot-pressed blends (Figure S18). For low-PVDF-content blends such as 20PVDF80NBR, the transverse piezoelectric coefficients are higher than the longitudinal piezoelectric coefficients, indicating a more sensitive stretching mode sensing performance than the compression mode.

2.4. Characterization of PVDF/NBR Sensors. To be used as a stretchable piezoelectric sensor, the electrode material must also have high stretchability. In this research, an electrically conductive nanocomposite consisting of multiwalled carbon nanotubes (MWCNTs), NBR, and photocuring agents was developed. This conductive nanocomposite electrode was formed by solvent evaporation from its suspension in a DMF/tetrahydrofuran (THF) mixed solvent, which was then cross-linked via a photocuring process according to the literature.[54] It should be noted that a fast-drying and photocurable electrode material is desired for piezoelectric sensors because it avoids additional high-temperature curing after application onto already electrically poled piezoelectric materials which may experience dielectric relaxation at the elevated temperature required for thermally cured electrodes. The stretchability and resistance of the MWCNTs/NBR electrode are shown in Figure S19, where the electrode can be stretched to 100% strain without any permanent damage. The Young's modulus of the MWCNTs/NBR nanocomposite is measured to be 14.5 MPa, which matches the Young's modulus of high-NBR-content PVDF/NBR blends like 20PVDF80NBR and ensures low overall stiffness of the sensors. After coating and curing the stretchable electrode on the poled PVDF/NBR, open-circuit voltage (V_{OC}) instead of charge (Q) was measured as the piezoelectric signal for sensing, due to a lower temperature sensitivity of V_{OC} near room temperature (Figure S20).

The PVDF/NBR piezoelectric sensors have two operation modes: stretching mode (g_{31} mode) and compression mode (g_{33}

https://doi.org/10.1021/acsami.3c01168
ACS Appl. Mater. Interfaces 2023, 15, 22320−22331

Table 1. Comparison of the Stretching Mode Piezoelectric PVDF/NBR Sensor in This Work with other Stretchable Piezoelectric Sensors

category	type	material	stretchability	maximum sensing strain	strain rate dependence	reference
pattern design	kirigami	PVDF film and PDMS		30%	yes	13
	kirigami	PVDF film and PET film	320%		yes	12
	serpentine structure	PVDF film and UV film		35%		11
	wavy structure	PVDF microfibers and VHB film	>350%		yes	8
	wavy structure	PVDF nanofibers and PDMS	110%	100%	yes	9
material design	nanocomposite	PZT/silicone	>200%	50%	yes	18
	nanocomposite	PZT/PDMS	254%			19
	nanocomposite	PMN-PT/MWCNTs/silicone	> 200%		yes	16
	nanocomposite	$BaTiO_3$/PDMS			yes	49
	sandwich composite	PVDF-TrFE nanofibers/PDMS	>30%			21
	polymer blend	PVDF/NBR	544%	70%	no	this work

mode). Stretching mode sensors are used for elongation and bending curvature measurements in wearable sensors or soft actuator calibrations where the dynamic excitation is in the transverse direction, so the 20PVDF80NBR blend is chosen based on its high stretchability, low modulus, and hysteresis. Figure 3 presents the characteristics of the stretching mode 20PVDF80NBR sensors including the working principle (Figure 3A). When subjected to a triangle wave strain excitation, the corresponding stress and voltage generation of a 20PVDF80NBR sensor were plotted in Figure 3B. Although the strain excitation is a linear triangle wave, the stress response is nonlinear due to viscoelasticity and hysteresis. The generated voltage follows a similar trend as the stress. At the end of the cycle, the unrecovered strain causes buckling (Figure 2D) which explains the negative stress and voltage due to slight compression. If only observing the first half-cycle and plotting the voltage against the stress and strain, it is clear that the generated voltage is proportional to the stress but has a nonlinear relationship with the strain (Figure 3C). This study reveals that although exhibiting nonlinearity with hysteresis, 20PVDF80NBR has sufficient stress transfer efficiency between the phases even under high strains because the piezoelectric voltage generated by the crystalline β phase PVDF is proportional to the apparent stress experienced by the entire polymer blend. However, the voltage−strain curve is nonlinear which is attributed to the nonlinear stress−strain curve of the polymer blend (Figure 2D). Next, the operating range of 20PVDF80NBR sensors was measured by repeatedly stretching a 20PVDF80NBR sensor to 100% strain. In Figure 3D, the 20PVDF80NBR sensor has a monotonic voltage−stress curve with an operating stress range up to 2.2 MPa, including a linear range up to 1.4 MPa. The voltage−strain curve is monotonic below 70% strain, indicating the maximum operating strain (ε_{op}) for strain sensing is 70% (Figure 3E). When the strain is above 70%, the generated voltage tends to saturate, which can be explained as an equilibrium between the voltage generation rate from the piezoelectric effect and the voltage draining rate based on the system time constant. Furthermore, the frequency dependence of the sensing behavior was investigated by using triangle wave excitations with various frequencies and amplitudes. Figure 3F shows the linear fitting slope of the voltage−stress (V-σ) response of a 20PVDF80NBR sensor under excitation frequencies from 0.25 to 4 Hz with a constant strain amplitude of 60%, which corresponds to strain rates ranging from 0.3 to 4.8 s^{-1}. The results show that the voltage−stress slope is frequency-independent and strain-rate-independent according to a one-way analysis of variance (ANOVA, p = 0.945). Similarly, the nonlinear voltage−strain response is also frequency and strain rate-insensitive for strains up to 60% (Figure 3G). Another test was performed on the same sensor with a fixed frequency of 0.5 Hz and various strain amplitudes, which corresponded to strain rates from 0.06 to 0.6 s^{-1}. In Figure 3H, all voltage−strain responses with different strain rates and strain amplitudes follow a consistent curve, confirming the strain rate independence of this sensor. In addition, the hysteresis study in Figure S21 shows that the 20PVDF80NBR sensor has negligible voltage−stress hysteresis, and its stress−strain and voltage−strain hysteresis decrease as the strain rate increases, making the sensor suitable for dynamic stress/strain measurements. Moreover, the influence of pre-stretch strain on the dynamic sensing performance was investigated by applying a dynamic sinusoidal strain excitation (Figure S22a) on a pre-stretched 20PVDF80NBR sensor. In Figure 3I, the measured voltage−stress slopes do not have significant dependence on the pre-stretch strain below 60% according to one-way ANOVA (p = 0.939), while the slope decreases as the pre-stretch strain exceeds 70%. On the other hand, the voltage−strain curves exhibit a consistent trend when the pre-stretch strain is below 50% (Figure 3J) but start having a significant dependence on the pre-stretch strain when it is above 60% (Figure S22b). Finally, the 20PVDF80NBR sensor was also shown to be capable of sensing small changes in stress and strain, such as dynamic strains as low as 0.15% (Figure S23). Therefore, stretching mode 20PVDF80NBR can be used as both stretchable strain and stress sensors that only require calibrations prior to operation, which can provide simple and repeatable dynamic strain/stress measurements with a 70% operating strain range. It also allows for highly reliable strain/stress sensing up to 50% strain with advantages such as strain rate independence and negligible pre-stretch influence. These unique features make the stretching mode PVDF/NBR blend an outstanding strain sensing material with intrinsic stretchability compared to other existing works (Table 1), especially under dynamic loading conditions. To further improve stretchability and operating strain range, smart pattern design can be applied to PVDF/NBR blend as the base material to fabricate ultrastretchable piezoelectric sensors in the future.

Compression mode sensors are used for tactile sensing, pressure, and normal force measurements, where the dynamic excitations are in the longitudinal direction. Considering the balance between transverse stretchability and longitudinal piezoelectric sensitivity (g_{33}), both 40PVDF60NBR and 20PVDF80NBR were tested as compression mode sensors in this research, yet 40PVDF60NBR was preferred for better

https://doi.org/10.1021/acsami.3c01168
ACS Appl. Mater. Interfaces 2023, 15, 22320−22331

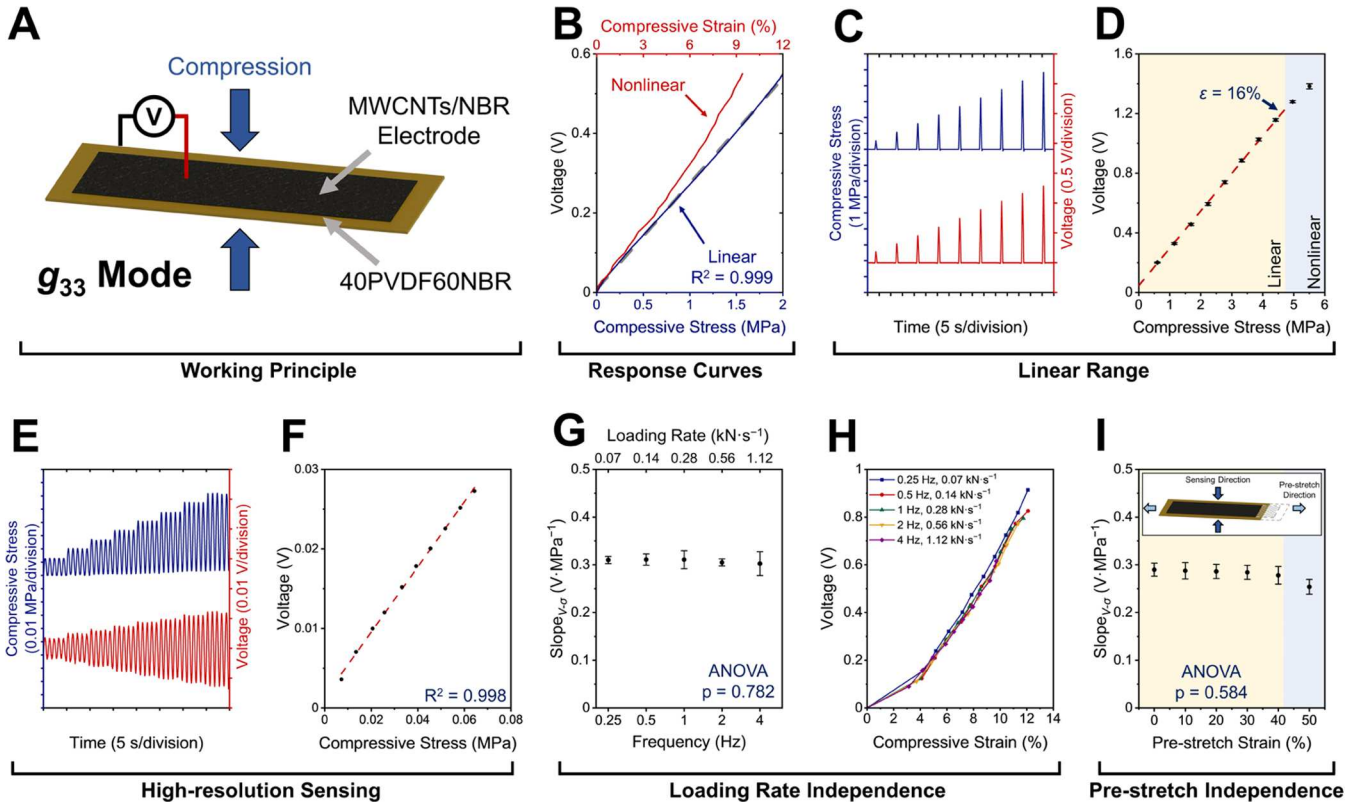

Figure 4. Characterization of the compression mode 40PVDF60NBR sensors. (A) Schematic of its working principle. (B) Voltage response with respect to stress and strain. (C) Voltage response to triangular compressive stresses with increasing amplitudes. (D) Linear range of the voltage−stress curves. (E) Voltage response to small-amplitude sinusoidal compressive stresses. (F) Linear voltage−stress relationship for small amplitudes. (G) Frequency- and loading-rate-independent voltage−stress slopes. (H) Frequency- and loading-rate-independent nonlinear voltage−strain curves. (I) Effect of transverse direction pre-stretch strain on longitudinal stress sensing.

sensitivity with moderate stretchability (274%). The characteristics of the 40PVDF60NBR compression mode sensors are presented in Figure 4 including the working principle (Figure 4A), while the characteristics of the more stretchable but less sensitive 20PVDF80NBR compression mode sensors are discussed in Figure S24 in the Supporting Information. It should be noted that during all compression tests, the two compression plates were never released from the sensor surfaces and a small compressive preload was always applied to the sensor to avoid any triboelectric effect. When a 40PVDF60NBR sensor was subjected to an increasing compressive load, the voltage−stress response was linear and the voltage−strain relationship was nonlinear (Figure 4B), which is attributed to the nonlinear compressive modulus. Moreover, for large-amplitude compressive stress sensing, a 40PVDF60NBR sensor was excited by triangular compressions with increasing amplitude, and the voltage generation aligned with the stress input after high-pass filtering out the low-frequency drift due to the time constant of the system (Figure 4C). By plotting peak voltages with respect to peak stresses (Figure 4D), the voltage is again proportional to the stress in the compression mode, with a linear range up to about 4.8 MPa compressive stress (corresponding compressive strain 16%). In addition, the resolution of its dynamic sensing ability was demonstrated by measuring the voltage output under small-amplitude sinusoidal compressive excitations (Figure 4E), which can be as low as 0.01 MPa. The various voltage amplitudes and stress amplitudes in this test were plotted in Figure 4F, and they could be well fitted by a linear function (R^2 = 0.998). Furthermore, the frequency and loading rate dependence of the compression mode 40PVDF60NBR was investigated by applying triangular compressive loads with different frequencies but a constant load amplitude. When under 0.25−4 Hz triangular compressive wave excitations, which correspond to loading rates from 0.07 to 1.12 kN s^{-1}, the slopes of the linear voltage−stress relationships show no significant dependence on the excitation frequency or loading rate according to one-way ANOVA (p = 0.782, Figure 4G). On the other hand, although the voltage−strain curves are nonlinear, they consistently follow the same trend regardless of frequency or loading rate (Figure 4H). Finally, the effect of transverse direction pre-stretch strain on longitudinal sensing performance was investigated by stretching a 40PVDF60NBR sensor to target strains and measuring the longitudinal piezoelectric responses simultaneously. From Figure 4I, it can be seen that the slope of voltage−stress relationships is almost identical when the pre-stretch strain is below 40%, which allows for reliable compression stress/force sensing even on stretched substrates. Thus, when used as a stress/force sensor in the compression mode, with only a voltage−stress slope calibration prior to operation, 40PVDF60NBR sensors can measure dynamic stress or force based on the voltage with high resolution and repeatability, which is also loading rate and pre-stretch insensitive.

2.5. Verification and Application of PVDF/NBR Sensors. To be used as reliable and accurate strain/stress sensors for various applications, PVDF/NBR sensors were bonded to multiple substrates to verify their sensing performance. The strain measurement accuracy of stretching mode 20PVDF80NBR sensors on three different materials was verified

https://doi.org/10.1021/acsami.3c01168
ACS Appl. Mater. Interfaces 2023, 15, 22320−22331

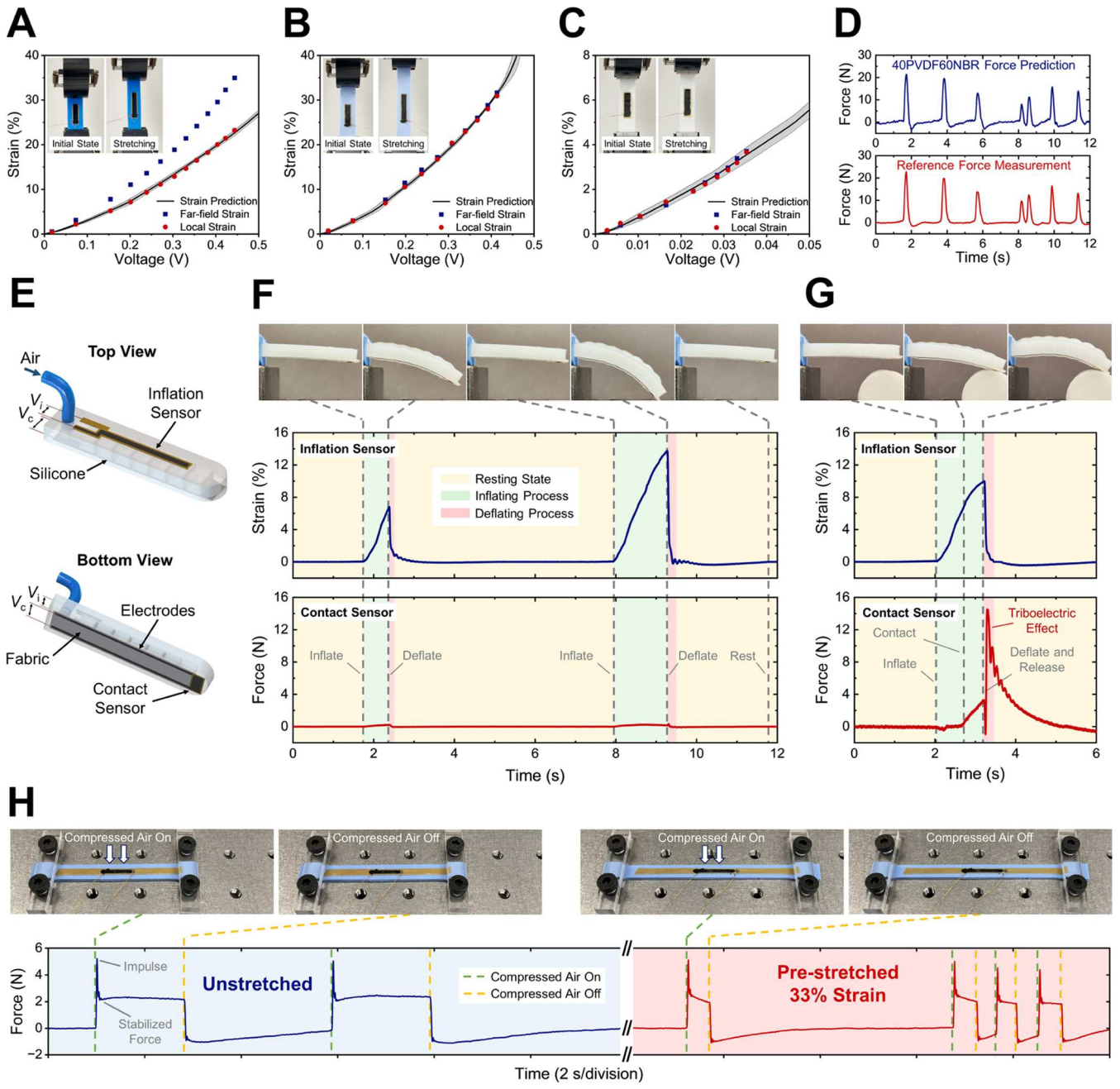

Figure 5. Verification and application of PVDF/NBR sensors. Strain verification of stretching mode 20PVDF80NBR sensors when bonded to: (A) Shore 30A silicone rubber, (B) Shore 62A silicone rubber, and (C) polyester fabric. (D) Force verification of a compression mode 40PVDF60NBR sensor when embedded in a silicone structure. (E) Schematics of a pneumatic soft actuator with an inflation sensor and a contact sensor. (F) Sensing demonstration in a free actuation case without any external load. (G) Sensing demonstration in a loaded actuation case. (H) Compression mode force sensing demonstration in unstretched and pre-stretched (33% strain) cases.

through digital image correlation (DIC). In Figure 5A, a 20PVDFNBR sensor was bonded to a soft silicone rubber (Shore 30A) by a silicone adhesive and tested uniaxially, and the voltage output was recorded to predict the tensile strain according to the previously calibrated voltage−strain curve for this sensor. The local strain under the sensor covered area measured by DIC agreed with the strain prediction using the voltage measurement, indicating a reliable local strain prediction after bonding to a substrate. However, the far-field strain of the soft silicone measured by the tensile test frame was always higher than the sensor local strain, which was caused by the modulus mismatch between the soft silicone and the sensor with adhesive. When a sensor was attached on a stiffer silicone rubber substrate (Shore 62A), not only the local strain but also the far-field strain matched the strain prediction based on voltage reading due to the lower sensor modulus than the substrate (Figure 5B). A 20PVDF80NBR sensor was also bonded to a less stretchable but porous polyester fabric to test a different type of substrate, and the strain prediction was verified by both the local and far-field strain measurements (Figure 5C). Thus, stretching mode 20PVDF80NBR sensors can accurately measure local strain of any substrates after bonding, without affecting the substrate strain distribution if substrates have comparable or higher modulus than the sensor and adhesive. For ultrasoft substrates,

https://doi.org/10.1021/acsami.3c01168
ACS Appl. Mater. Interfaces 2023, 15, 22320−22331

sensors made of higher-NBR-content blends (e.g., 10PVDF90NBR) can be fabricated and bonded with softer silicone adhesives. The stress (or force) measurement accuracy of a compression mode 40PVDF60NBR sensor embedded in soft structures was verified based on a commercial piezoceramic force sensor. It should be noted that only force is directly measurable because of unknown contact area. When applying external forces to a 40PVDF60NBR sensor in a silicone structure on top of a fixed piezoceramic force sensor (Figure S25), the force predicted by the 40PVDF60NBR sensor, and the same force measured by the piezoceramic force sensor is shown in Figure 5D. The force prediction and reference measurement are in close agreement with each other, while some slight distinctions still exist due to the contact surface alignment error and discharging time constant difference between the two sensors. Similarly, the force measurement verification of a compression mode 20PVDF80NBR sensor is presented in Figure S26. In general, the verification results confirm that these two modes of PVDF/NBR sensors can be used on soft structures for reliable strain and force measurements.

Furthermore, a 20PVDF80NBR inflation sensor (stretching mode) on the top and a 40PVDF60NBR contact sensor (compression mode) on the bottom of a finger-shaped pneumatic soft actuator (Figure 5E) demonstrated the application of stretchable PVDF/NBR sensors. Two open-circuit voltages, V_i and V_c, were measured from the inflation sensor and contact sensor, respectively, and then were used to calculate the top surface inflation strain and bottom tip contact force based on calibration curves. Figure 5F shows a free actuation case without any external load, where the actuator was inflated and deflated twice with different inflating times (Movie S2). The inflation sensor had active strain measurements when it was stretched during the inflation process, and its strain measurements tracked the two different bending curvatures. On the other hand, the contact sensor on the less stretchable bottom surface showed negligible force change during the inflating and deflating cycles, which was caused by the voltage generation from unavoidable bottom surface stretching in the transverse direction and undesirable wire vibration-induced high-impedance voltage change. Figure 5G shows a loaded actuation case, where the actuator was inflated, blocked by a cylindrical obstacle, and deflated (Movie S3). In this case, the inflation sensor picked up a change in strain as the inflating process began, and then had a reduction in strain rate after the actuator touched the obstacle. Though having a similar inflating time, the peak strain in the loaded actuation case was lower than the second inflating cycle in the free actuation case, indicating a decreased bending curvature due to the blockage. The tip contact sensor started showing significant force reading after the actuator touched the obstacle, and the force exerted on the contact sensor went up as the inflating process continued. It should be noted that at the time of deflation, the actuator was suddenly released from the obstacle, causing a strong voltage spike in the contact sensor measurement due to the triboelectric effect (Section 8.2 in the Supporting Information). This resulted in a meaningless force prediction from the contact sensor right after it was detached from the obstacle.

To further demonstrate the force sensing capability of stretchable compression mode PVDF/NBR sensors, a 40PVDF60NBR sensor bonded to a Shore 62A silicone was tested with and without transverse pre-stretch strains. A compressed air source with a constant pressure was used as the longitudinal force excitation to the sensor, which had no direct contact with the sensor surface to avoid triboelectric effect. In Figure 5H, at the moment when the compressed air was turned on, a sudden spike of force (~4 N) was measured by the sensor due to the impulse, followed by a stabilized force of 2 N with slow decay due to the constant air pressure. When the compressed air was turned off, a sudden drop in force reading followed by slow decay was observed. Comparing the force measurements in both unstretched and pre-stretched (33% strain) cases, the peak impulse force and the stabilized force are consistent, confirming a reliable force measurement from the sensor regardless of the pre-stretch strain. The main difference between the two cases is the signal decay rate, which is caused by the change of sensor capacitance and resistance after stretching. In general, the stretchable PVDF/NBR sensors demonstrate promising dynamic strain and stress (force) sensing capabilities for soft structures, while additional methods to remove triboelectric contribution such as flexible shielding[55] and using flexible electronics[56,57] to enable in situ signal conditioning are needed for future practical operations.

3. CONCLUSIONS

A novel stretchable piezoelectric PVDF/NBR polymer blend is produced through precipitation printing then hot pressing for vulcanization, which exhibits strong β phase PVDF, a blend morphology of submicron-level phase separation, and a high stretchability up to 544%. The resulting PVDF/NBR blend can be considered as a continuous elastomer phase above the micron scale, which behaves like rubber and is different from typical two-phase piezoelectric nanocomposites. After electric poling and adding stretchable electrodes, the PVDF/NBR blend shows outstanding piezoelectric properties, which can be used as both stretchable dynamic strain (stretching mode) and stress (compression mode) sensors. The stretching mode 20PVDF80NBR sensors have an operating sensing range up to 70% strain, which is strain-rate-independent in the range from 0.06 to 4.8 s^{-1} and insensitive to pre-stretch up to 50% strain. The compression mode 40PVDF60NBR sensors have a linear voltage−stress relationship below 4.8 MPa stress, with loading rate independence in the range from 0.07 to 1.12 kN s^{-1} and transverse pre-stretch independence up to 40% strain. Based on these advantages, the two demonstrations of the pneumatic soft actuator with two sensors and the sensor on a pre-stretched soft substrate show the potential application of PVDF/NBR sensors for reliable and accurate sensing of stretchable structures under dynamic loading conditions, which can be used for wearable sensing devices, soft actuator calibration, and soft robot control.

4. EXPERIMENTAL SECTION

4.1. PVDF/NBR Printing Ink Preparation. PVDF powder (Kynar 301F) was first dissolved in DMF (ACS certified, Fisher Chemical) to form a 15 wt % clear solution (100PVDF ink) via magnetic stirring and sonication (Branson M2800), while unvulcanized NBR (KNB 40M, Kumho Petrochemical) was also dissolved in DMF to form a 15 wt % uniform but opaque solution via sonication (sonic dismembrator model 500, Fisher Scientific). 1 wt % sulfur (Akrochem) and 1 wt % *N*-cyclohexyl-2-benzothioazole sulfenamide (Accelerator CBTS, Akrochem) based on the NBR solid weight were added into the NBR/DMF solution for further mixing to obtain 100NBR ink. For different ratios of PVDF/NBR blend inks, 100PVDF and 100NBR inks were mixed based on the corresponding weight ratios, followed by vortex mixing.

4.2. MWCNTs/NBR Conductive Paste Preparation. First, 0.87 g of unvulcanized NBR was dissolved in 3.48 g of DMF via sonication. Then, 8.08 g of THF (ACS certified, Fisher Chemical) was added to the solution and mixed again. Next, 0.13 g of MWCNTs (Cheap Tubes)

https://doi.org/10.1021/acsami.3c01168
ACS Appl. Mater. Interfaces 2023, 15, 22320−22331

were added into the solution and dispersed uniformly through sonication and magnetic stirring to form a conductive paste. Before painting the electrodes, 87 mg of trimethylolpropane tris(3-mercaptopropionate) (Sigma-Aldrich) and 17 mg of diphenyl(2,4,6-trimethylbenzoyl)phosphine oxide (Sigma-Aldrich) were also added to the paste for subsequent photocuring.

4.3. PVDF/NBR Piezoelectric Sensor Fabrication. Prepared PVDF/NBR printing inks were precipitation-printed inside an ice/water mixture bath with a 24-gauge nozzle, 7 mm s^{-1} printing speed, and 3−4.5 psi pressure (Table S5), using a gantry system (AGS1500, Aerotech) and a high-precision dispenser (Ultimus V, Nordson EFD). After precipitation printing, rectangular shape samples (thickness ranging from 0.2 to 1.5 mm) were dried at 80 °C for 4 h to remove residual water and DMF inside the samples. Subsequent hot pressing was performed on the rectangular shape samples at 150 °C and 0.5−60 MPa (Table S5) for 2 h to reduce the porosity of the samples and induce vulcanization at the same time. Direct contact electric poling was applied to hot-pressed samples using flat aluminum blocks as electrodes in an 80 °C oil bath. The poling electric field strength was set to be the highest before breakdown for different types of samples (Table S2), ranging from 30 to 100 MV m^{-1}. After poling, both sides of the PVDF/NBR piezoelectric sensors were painted with the prepared MWCNT/NBR conductive paste, which was dried at room temperature for 4 h and UV-light-cured to form highly stretchable electrodes.

4.4. Characterization and Testing Methods. The detailed characterization and testing procedures, setups, and methods are provided in Section 9.2 in the Supporting Information and Figure S27.

■ ASSOCIATED CONTENT

Supporting Information

The Supporting Information is available free of charge at https://pubs.acs.org/doi/10.1021/acsami.3c01168.

Details of supplementary findings and testing methods (PDF)

Stretching 20PVDF80NBR (Movie S1) (mp4)

Soft Actuator Free Actuation (Movie S2) (mp4)

Soft Actuator Loaded Actuation (Movie S3) (mp4)

■ AUTHOR INFORMATION

Corresponding Author

Henry A. Sodano − *Department of Aerospace Engineering, University of Michigan, Ann Arbor, Michigan 48109, United States; Department of Materials Science and Engineering and Department of Macromolecular Science and Engineering, University of Michigan, Ann Arbor, Michigan 48109, United States;* orcid.org/0000-0001-6269-1802; Email: hsodano@umich.edu

Author

Ruowen Tu − *Department of Aerospace Engineering, University of Michigan, Ann Arbor, Michigan 48109, United States;* orcid.org/0000-0003-2681-8030

Complete contact information is available at: https://pubs.acs.org/10.1021/acsami.3c01168

Author Contributions

R.T.: Conceptualization, investigation, methodology, and writing—original draft. H.A.S.: Conceptualization, supervision, funding acquisition, writing—review & editing. All authors have given approval to the final version of the manuscript.

Funding

National Science Foundation under Grant # EFRI-1935216.

Notes

The authors declare no competing financial interest.

■ ACKNOWLEDGMENTS

The authors gratefully acknowledge support for this work from the National Science Foundation under Grant # EFRI-1935216.

■ REFERENCES

(1) Wang, X.; Liu, Z.; Zhang, T. Flexible Sensing Electronics for Wearable/Attachable Health Monitoring. *Small* **2017**, *13*, No. 1602790.

(2) Amjadi, M.; Kyung, K.-U.; Park, I.; Sitti, M. Stretchable, Skin-Mountable, and Wearable Strain Sensors and Their Potential Applications: A Review. *Adv. Funct. Mater.* **2016**, *26*, 1678−1698.

(3) Mengüç, Y.; Park, Y.-L.; Martinez-Villalpando, E.; Aubin, P.; Zisook, M.; Stirling, L.; Wood, R. J.; Walsh, C. J. Soft Wearable Motion Sensing Suit for Lower Limb Biomechanics Measurements. *2013 IEEE Int. Conf. Rob. Autom.* **2013**, 5309−5316.

(4) Park, W.; Ro, K.; Kim, S.; Bae, J. A Soft Sensor-Based Three-Dimensional (3-D) Finger Motion Measurement System. *Sensors* **2017**, *17*, 420.

(5) Lu, N.; Kim, D.-H. Flexible and Stretchable Electronics Paving the Way for Soft Robotics. *Soft Rob.* **2014**, *1*, 53−62.

(6) Souri, H.; Banerjee, H.; Jusufi, A.; Radacsi, N.; Stokes, A. A.; Park, I.; Sitti, M.; Amjadi, M. Wearable and Stretchable Strain Sensors: Materials, Sensing Mechanisms, and Applications. *Adv. Intell. Syst.* **2020**, *2*, No. 2000039.

(7) Kim, D.-H.; Song, J.; Choi, W. M.; Kim, H.-S.; Kim, R.-H.; Liu, Z.; Huang, Y. Y.; Hwang, K.-C.; Zhang, Y.; Rogers, J. A. Materials and Noncoplanar Mesh Designs for Integrated Circuits with Linear Elastic Responses to Extreme Mechanical Deformations. *Proc. Natl. Acad. Sci. U.S.A.* **2008**, *105*, 18675−18680.

(8) Yuan, Y.; Dai, Y.; Xu, M.; Wang, Z.; Chen, Z. Highly Stretchable Piezoelectric Strain Sensor With Dual Wavy Structures of PVDF Microfibers. *2020 IEEE 4th Info. Technol., Networking, Electron. Autom. Control Conf. (ITNEC)* **2020**, *1*, 2418−2422.

(9) Duan, Y.; Huang, Y.; Yin, Z.; Bu, N.; Dong, W. Non-Wrinkled, Highly Stretchable Piezoelectric Devices by Electrohydrodynamic Direct-Writing. *Nanoscale* **2014**, *6*, 3289−3295.

(10) Xu, S.; Zhang, Y.; Cho, J.; Lee, J.; Huang, X.; Jia, L.; Fan, J. A.; Su, Y.; Su, J.; Zhang, H.; Cheng, H.; Lu, B.; Yu, C.; Chuang, C.; Kim, T.; Song, T.; Shigeta, K.; Kang, S.; Dagdeviren, C.; Petrov, I.; Braun, P. V.; Huang, Y.; Paik, U.; Rogers, J. A. Stretchable Batteries with Self-Similar Serpentine Interconnects and Integrated Wireless Recharging Systems. *Nat. Commun.* **2013**, *4*, No. 1543.

(11) Ji, Z.; Zhang, M. Highly Sensitive and Stretchable Piezoelectric Strain Sensor Enabled Wearable Devices for Real-Time Monitoring of Respiratory and Heartbeat Simultaneously. *Nanotechnol. Precis. Eng.* **2022**, *5*, No. 013002.

(12) Kim, Y.-G.; Song, J.-H.; Hong, S.; Ahn, S.-H. Piezoelectric Strain Sensor with High Sensitivity and High Stretchability Based on Kirigami Design Cutting. *npj Flexible Electron.* **2022**, *6*, No. 52.

(13) Sun, R.; Carreira, S. C.; Chen, Y.; Xiang, C.; Xu, L.; Zhang, B.; Chen, M.; Farrow, I.; Scarpa, F.; Rossiter, J. Stretchable Piezoelectric Sensing Systems for Self-Powered and Wireless Health Monitoring. *Adv. Mater. Technol.* **2019**, *4*, No. 1900100.

(14) Dagdeviren, C.; Joe, P.; Tuzman, O. L.; Park, K.-I.; Lee, K. J.; Shi, Y.; Huang, Y.; Rogers, J. A. Recent Progress in Flexible and Stretchable Piezoelectric Devices for Mechanical Energy Harvesting, Sensing and Actuation. *Extreme Mech. Lett.* **2016**, *9*, 269−281.

(15) Zhou, H.; Zhang, Y.; Qiu, Y.; Wu, H.; Qin, W.; Liao, Y.; Yu, Q.; Cheng, H. Stretchable Piezoelectric Energy Harvesters and Self-Powered Sensors for Wearable and Implantable Devices. *Biosens. Bioelectron.* **2020**, *168*, No. 112569.

(16) Jeong, C. K.; Lee, J.; Han, S.; Ryu, J.; Hwang, G.-T.; Park, D. Y.; Park, J. H.; Lee, S. S.; Byun, M.; Ko, S. H.; Lee, K. J. A Hyper-Stretchable Elastic-Composite Energy Harvester. *Adv. Mater.* **2015**, *27*, 2866−2875.

(17) Wu, W.; Bai, S.; Yuan, M.; Qin, Y.; Wang, Z. L.; Jing, T. Lead Zirconate Titanate Nanowire Textile Nanogenerator for Wearable

Energy-Harvesting and Self-Powered Devices. *ACS Nano* **2012**, *6*, 6231−6235.
(18) Chou, X.; Zhu, J.; Qian, S.; Niu, X.; Qian, J.; Hou, X.; Mu, J.; Geng, W.; Cho, J.; He, J.; Xue, C. All-in-One Filler-Elastomer-Based High-Performance Stretchable Piezoelectric Nanogenerator for Kinetic Energy Harvesting and Self-Powered Motion Monitoring. *Nano Energy* **2018**, *53*, 550−558.
(19) Quinsaat, J. E. Q.; de Wild, T.; Nüesch, F. A.; Damjanovic, D.; Krämer, R.; Schürch, G.; Häfliger, D.; Clemens, F.; Sebastian, T.; Dascalu, M.; Opris, D. M. Stretchable Piezoelectric Elastic Composites for Sensors and Energy Generators. *Composites, Part B* **2020**, *198*, No. 108211.
(20) He, Z.; Rault, F.; Lewandowski, M.; Mohsenzadeh, E.; Salaün, F. Electrospun PVDF Nanofibers for Piezoelectric Applications: A Review of the Influence of Electrospinning Parameters on the β Phase and Crystallinity Enhancement. *Polymers* **2021**, *13*, 174.
(21) Park, S.-H.; Lee, H. B.; Yeon, S. M.; Park, J.; Lee, N. K. Flexible and Stretchable Piezoelectric Sensor with Thickness-Tunable Configuration of Electrospun Nanofiber Mat and Elastomeric Substrates. *ACS Appl. Mater. Interfaces* **2016**, *8*, 24773−24781.
(22) Siddiqui, S.; Kim, D.-I.; Roh, E.; Duy, L. T.; Trung, T. Q.; Nguyen, M. T.; Lee, N.-E. A Durable and Stable Piezoelectric Nanogenerator with Nanocomposite Nanofibers Embedded in an Elastomer under High Loading for a Self-Powered Sensor System. *Nano Energy* **2016**, *30*, 434−442.
(23) Elashmawi, Is.; Hakeem, Na. Effect of PMMA Addition on Characterization and Morphology of PVDF. *Polym. Eng. Sci.* **2008**, *48*, 895−901.
(24) Kang, S. J.; Park, Y. J.; Bae, I.; Kim, K. J.; Kim, H.-C.; Bauer, S.; Thomas, E. L.; Park, C. Printable Ferroelectric PVDF/PMMA Blend Films with Ultralow Roughness for Low Voltage Non-Volatile Polymer Memory. *Adv. Funct. Mater.* **2009**, *19*, 2812−2818.
(25) Leppe-Nerey, J. R.; Nicho, M. E.; Sierra-Espinosa, F. Z.; Hernández-Guzmán, F.; Fuentes-Pérez, M. Experimental Study of Piezoelectric Polymeric Film as Energy Harvester. *Mater. Sci. Eng. B* **2021**, *272*, No. 115366.
(26) Valadorou, D.; Papathanassiou, A. N.; Kolonelou, E.; Sakellis, E. Boosting the Electro-Mechanical Coupling of Piezoelectric Polyvinyl Alcohol−Polyvinylidene Fluoride Blends by Dispersing Nano-Graphene Platelets. *J. Phys. D: Appl. Phys.* **2022**, *55*, No. 295501.
(27) Shehata, N.; Nair, R.; Boualayan, R.; Kandas, I.; Masrani, A.; Elnabawy, E.; Omran, N.; Gamal, M.; Hassanin, A. H. Stretchable Nanofibers of Polyvinylidenefluoride (PVDF)/Thermoplastic Polyurethane (TPU) Nanocomposite to Support Piezoelectric Response via Mechanical Elasticity. *Sci. Rep.* **2022**, *12*, No. 8335.
(28) Kim, H.; Manriquez, L. C. D.; Islam, M. T.; Chavez, L. A.; Regis, J. E.; Ahsan, M. A.; Noveron, J. C.; Tseng, T.-L. B.; Lin, Y. 3D Printing of Polyvinylidene Fluoride/Photopolymer Resin Blends for Piezoelectric Pressure Sensing Application Using the Stereolithography Technique. *MRS Commun.* **2019**, *9*, 1115−1123.
(29) Xu, C.; Wang, Y.; Chen, Y. Highly Toughened Poly(Vinylidene Fluoride)/Nitrile Butadiene Rubber Blends Prepared via Peroxide-Induced Dynamic Vulcanization. *Polym. Test.* **2014**, *33*, 179−186.
(30) Jiang, X.; Xu, C.; Wang, Y.; Chen, Y. Polyvinylidene Fluoride/Acrylonitrile Butadiene Rubber Blends Prepared Via Dynamic Vulcanization. *J. Macromol. Sci., Part B* **2015**, *54*, 58−70.
(31) Tu, R.; Sprague, E.; Sodano, H. A. Precipitation Printing towards Diverse Materials, Mechanical Tailoring and Functional Devices. *Addit. Manuf.* **2020**, *35*, No. 101358.
(32) Zhang, M.; Zhang, A.-Q.; Zhu, B.-K.; Du, C.-H.; Xu, Y.-Y. Polymorphism in Porous Poly(Vinylidene Fluoride) Membranes Formed via Immersion Precipitation Process. *J. Membr. Sci.* **2008**, *319*, 169−175.
(33) Wang, X.; Zhang, L.; Sun, D.; An, Q.; Chen, H. Formation Mechanism and Crystallization of Poly(Vinylidene Fluoride) Membrane via Immersion Precipitation Method. *Desalination* **2009**, *236*, 170−178.
(34) Cheng, L.-P. Effect of Temperature on the Formation of Microporous PVDF Membranes by Precipitation from 1-Octanol/DMF/PVDF and Water/DMF/PVDF Systems. *Macromolecules* **1999**, *32*, 6668−6674.
(35) Tu, R.; Sprague, E.; Sodano, H. A. Precipitation-Printed High-β Phase Poly(Vinylidene Fluoride) for Energy Harvesting. *ACS Appl. Mater. Interfaces* **2020**, *12*, 58072−58081.
(36) Chen, S.; Wei, Y.; Yuan, X.; Lin, Y.; Liu, L. A Highly Stretchable Strain Sensor Based on a Graphene/Silver Nanoparticle Synergic Conductive Network and a Sandwich Structure. *J. Mater. Chem. C* **2016**, *4*, 4304−4311.
(37) Li, Y.; Zhou, B.; Zheng, G.; Liu, X.; Li, T.; Yan, C.; Cheng, C.; Dai, K.; Liu, C.; Shen, C.; Guo, Z. Continuously Prepared Highly Conductive and Stretchable SWNT/MWNT Synergistically Composited Electrospun Thermoplastic Polyurethane Yarns for Wearable Sensing. *J. Mater. Chem. C* **2018**, *6*, 2258−2269.
(38) Lin, Y.; Dong, X.; Liu, S.; Chen, S.; Wei, Y.; Liu, L. Graphene−Elastomer Composites with Segregated Nanostructured Network for Liquid and Strain Sensing Application. *ACS Appl. Mater. Interfaces* **2016**, *8*, 24143−24151.
(39) Yang, H.; Yao, X.; Zheng, Z.; Gong, L.; Yuan, L.; Yuan, Y.; Liu, Y. Highly Sensitive and Stretchable Graphene-Silicone Rubber Composites for Strain Sensing. *Compos. Sci. Technol.* **2018**, *167*, 371−378.
(40) Liu, X.; Liang, X.; Lin, Z.; Lei, Z.; Xiong, Y.; Hu, Y.; Zhu, P.; Sun, R.; Wong, C.-P. Highly Sensitive and Stretchable Strain Sensor Based on a Synergistic Hybrid Conductive Network. *ACS Appl. Mater. Interfaces* **2020**, *12*, 42420−42429.
(41) Wang, L.; Chen, Y.; Lin, L.; Wang, H.; Huang, X.; Xue, H.; Gao, J. Highly Stretchable, Anti-Corrosive and Wearable Strain Sensors Based on the PDMS/CNTs Decorated Elastomer Nanofiber Composite. *Chem. Eng. J.* **2019**, *362*, 89−98.
(42) Ko, H.-U.; Kim, H. C.; Kim, J. W.; Park, J.; Kim, J. Soft Piezoelectric Polymer of Poly[Di(Ethylene Glycol) Adipate] Plasticized Poly Vinyl Chloride and Its Strain Sensing. *Mater. Lett.* **2018**, *227*, 276−280.
(43) Soin, N.; Boyer, D.; Prashanthi, K.; Sharma, S.; Narasimulu, A. A.; Luo, J.; Shah, T. H.; Siores, E.; Thundat, T. Exclusive Self-Aligned β-Phase PVDF Films with Abnormal Piezoelectric Coefficient Prepared via Phase Inversion. *Chem. Commun.* **2015**, *51*, 8257−8260.
(44) Fortunato, M.; Cavallini, D.; De Bellis, G.; Marra, F.; Tamburrano, A.; Sarto, F.; Sarto, M. S. Phase Inversion in PVDF Films with Enhanced Piezoresponse Through Spin-Coating and Quenching. *Polymers* **2019**, *11*, 1096.
(45) Cai, X.; Lei, T.; Sun, D.; Lin, L. A Critical Analysis of the α, β and γ Phases in Poly(Vinylidene Fluoride) Using FTIR. *RSC Adv.* **2017**, *7*, 15382−15389.
(46) Lei, T.; Cai, X.; Wang, X.; Yu, L.; Hu, X.; Zheng, G.; Lv, W.; Wang, L.; Wu, D.; Sun, D.; Lin, L. Spectroscopic Evidence for a High Fraction of Ferroelectric Phase Induced in Electrospun Polyvinylidene Fluoride Fibers. *RSC Adv.* **2013**, *3*, 24952−24958.
(47) Esterly, D. M.; Love, B. J. Phase Transformation to β-Poly(Vinylidene Fluoride) by Milling. *J. Polym. Sci., Part B: Polym. Phys.* **2004**, *42*, 91−97.
(48) Boom, Rm.; Rolevink, H. w. w.; Boomgaard van den, Th.; Smolders, Ca. Microscopic Structures in Phase Inversion Membranes: The Use of Polymer Blends for Membrane Formation by Immersion Precipitation. *Makromol. Chem., Macromol. Symp.* **1993**, *69*, 133−140.
(49) Park, K.-I.; Bin Bae, S.; Ho Yang, S.; Ik Lee, H.; Lee, K.; Jun Lee, S. Lead-Free BaTiO 3 Nanowires-Based Flexible Nanocomposite Generator. *Nanoscale* **2014**, *6*, 8962−8968.
(50) Laiarinandrasana, L.; Besson, J.; Lafarge, M.; Hochstetter, G. Temperature Dependent Mechanical Behaviour of PVDF: Experiments and Numerical Modelling. *Int. J. Plast.* **2009**, *25*, 1301−1324.
(51) Thakur, Y.; Zhang, B.; Dong, R.; Lu, W.; Iacob, C.; Runt, J.; Bernholc, J.; Zhang, Q. M. Generating High Dielectric Constant Blends from Lower Dielectric Constant Dipolar Polymers Using Nanostructure Engineering. *Nano Energy* **2017**, *32*, 73−79.
(52) Janik, P.; Paluch, M.; Ziolo, J.; Sulkowski, W.; Nikiel, L. Low-Frequency Dielectric Relaxation in Rubber. *Phys. Rev. E* **2001**, *64*, No. 042502.

https://doi.org/10.1021/acsami.3c01168
ACS Appl. Mater. Interfaces 2023, 15, 22320−22331

(53) Abd-El-Messieh, S. L.; Younan, A. F. Dielectric Relaxation and Mechanical Properties of Natural and Chloroprene Rubber with Some Nitroaniline Additives. *J. Appl. Polym. Sci.* **1996**, *62*, 805−812.
(54) Decker, C.; Viet, T. N. T. Photocrosslinking of Functionalized Rubbers, 8. The Thiol-Polybutadiene System. *Macromol. Chem. Phys.* **1999**, *200*, 1965−1974.
(55) Chen, C.; Zhao, S.; Pan, C.; Zi, Y.; Wang, F.; Yang, C.; Wang, Z. L. A Method for Quantitatively Separating the Piezoelectric Component from the As-Received "Piezoelectric" Signal. *Nat. Commun.* **2022**, *13*, No. 1391.
(56) Gao, W.; Ota, H.; Kiriya, D.; Takei, K.; Javey, A. Flexible Electronics toward Wearable Sensing. *Acc. Chem. Res.* **2019**, *52*, 523−533.
(57) Wang, P.; Hu, M.; Wang, H.; Chen, Z.; Feng, Y.; Wang, J.; Ling, W.; Huang, Y. The Evolution of Flexible Electronics: From Nature, Beyond Nature, and To Nature. *Adv. Sci.* **2020**, *7*, No. 2001116.

https://doi.org/10.1021/acsami.3c01168
ACS Appl. Mater. Interfaces 2023, 15, 22320−22331